

Design of infrared non-destructive testing for damage detection in multi-layer materials

by E. Borazjani*, D. Spinello* and D. Neculescu*

*Dept. of Mechanical Engineering, University of Ottawa, 161 Louis Pasteur Pvt, Ottawa, K1N 6N5 Canada, {ebora085, dspinell, necsu}@uottawa.ca

Abstract -The inverse heat conduction in a multi-material slab with periodic temperature excitation is investigated. We derive a polynomial relation to estimate the frequency of the periodic excitation as a function of the temperature amplitude at a given observation point in the material specimen. The formula includes characteristic geometric and material parameters of the system. The polynomial formula can be an effective design tool for quick frequency predetermination in the design of non-destructive testing experiments with infrared thermography. The convergence and accuracy of the formula are assessed by comparison with analytical thermal quadrupoles solution.

1. Introduction

Infrared thermography is a non-destructive testing technique in the field of failure detection. Material, civil and aerospace engineering are some of the application areas of infrared thermography [1], [2], [3]. The inspection becomes more challenging for composite and multi-layer materials especially in the field of aerospace [4]. Any defect in multi-layer material or composite such as ply separation, air bubbles and delimitation can lead to the modification of their properties [5], which can affect reliability and safety. Detecting a characteristic of a possible defect in a shorter time and easier way are two notable benefit of infrared thermography [6]. This method can be applied in two different ways, namely active and passive thermography [7].

In active infrared thermography, the specimen is excited by an external thermal heat source and a camera captures the images. The images are processed by computers and any lack of integrity on the surface or inside the structure is detected. Several parameters are involved in detection techniques to have clear and accurate results, such as material properties of tested objects and depth and size of the defect [8]. Active infrared thermography requires the experimental setup design. Effective experimental design requires the predetermination of the radial frequency of the boundary excitation that corresponds to certain temperature amplitude, since this parameter is correlated with the size and characteristics of the flaws [8].

A closed form solution of the inverse problem was derived in [9] for a semi-infinite domain. The applicability and limitation of this formula were assessed in [10]. Here we consider the inverse problem for a multi-layer heat conducting solid. We use the thermal quadrupoles representation to derive a lumped parameters formulation of the problem that allows for the input to output representation in terms of a transfer function in the Laplace domain. The generally transcendental transfer function is approximated with the corresponding power series, which allows for a polynomial implicit approximated solution of the inverse problem. Explicit approximate solutions are given up to third order truncation.

The rest of the paper is organized as follows. In Section 2 we briefly recall the formulation of the initial-boundary values problem describing the heat conduction in a multi-layer slab with periodic temperature excitation. In Section 3 we introduce a lumped parameters representation of the problem by means of thermal quadrupoles [11]. In Section 4 we derive an implicit approximated formula that solves the inverse problem (determination of the frequency of excitation given the amplitude of the temperature at a given observation point) for design of experiments in nondestructive testing of bi-material slabs. The formula includes characteristic geometric and material parameters of the bi-material system. The accuracy of the formula with respect to analytical results of the direct problem, and convergence of the polynomial solution with increasing truncation order is established. Section 5 summarizes the results and contributions.

2. Heat conduction in a two-layer slab

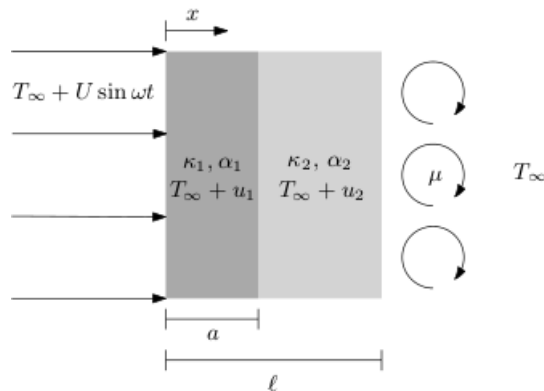


Fig. 1. Schematics of a two-layers slab with temperature radiation on one side and convection on the other side. Here T_∞ is a uniform ambient temperature.

We consider a multi-layer slab-like domain, see figure 1, which is a three dimensional continuum with two sides very large with respect to thickness so that the effect of the edges can be neglected. It is therefore appropriate to introduce a reduced one-dimensional approximation along the spatial coordinate $x \in [0, \ell]$ of the initial boundary values problem governing the heat conduction. Moreover, we assume that the lateral surface has no heat loss and that there is no internal heat source, and formulate the one-dimensional initial-boundary values heat conduction problem as

$$\frac{\partial u_i}{\partial t} = \alpha_i \frac{\partial^2 u_i}{\partial x^2}, \quad i = 1, 2, \dots, n \tag{1a}$$

$$u_i(x, 0) = 0 \tag{1b}$$

$$u_i(a_i, t) = u_{i+1}(a_i, t), \quad i = 1, 2, \dots, n - 1 \tag{1c}$$

$$k_i \frac{\partial u_i}{\partial x}(a_i, t) = k_{i+1} \frac{\partial u_{i+1}}{\partial x}(a_i, t), \quad i = 1, 2, \dots, n - 1 \tag{1d}$$

$$u_1(0, t) = U \sin \omega t \tag{1e}$$

$$k_n \frac{\partial u_n}{\partial x}(\ell, t) = -\mu u_n(\ell, t) \tag{1f}$$

where u_i is the temperature raise (with respect to the ambient temperature) in the i -th layer at point $(x, t) \in \mathbb{R} \times \mathbb{R}$, a_1, a_2, \dots, a_{n-1} are the coordinates of the material interfaces in the slab that are assumed to be parallel to the sides at $x = 0$ and $x = \ell$, and constants α_i and k_i represent respectively the thermal diffusivity and the thermal conductivity of the materials. We consider $a_0 \equiv 0$ and $a_n \equiv \ell$. The slab is assumed to be initially at the ambient temperature consistently with the initial condition (1b). At time zero a persistent oscillating perturbation of amplitude U and radian frequency ω is added at $x = 0$, as formalized by the boundary condition (1e). Equation (1f) is a convective boundary condition describing the experimental conditions that we want to reproduce. By introducing the non-dimensional variables

$$u_i^* = \frac{u_i}{U}, \quad x^* = \frac{x}{\ell}, \quad t^* = \omega t$$

we rewrite the initial-boundary values problem (1) in the non-dimensional form

$$\frac{\partial u_i^*}{\partial t^*} = \frac{1}{\beta_i} \frac{\partial^2 u_i^*}{\partial x^{*2}} \tag{2a}$$

$$u_i^*(x^*, 0) = 0 \tag{2b}$$

$$u_i^*(a_i^*, t^*) = u_{i+1}^*(a_i^*, t^*) \tag{2c}$$

$$\rho_i \frac{\partial u_i^*}{\partial x^*}(a_i^*, t^*) = \rho_{i+1} \frac{\partial u_{i+1}^*}{\partial x^*}(a_i^*, t^*) \tag{2d}$$

$$u_1^*(0, t^*) = \sin t^* \tag{2e}$$

$$\frac{\partial u_n^*}{\partial x^*}(1, t^*) + \sigma u_n^*(1, t^*) = 0 \tag{2f}$$

with the nondimensional groups defined by

$$\beta_i = \frac{\omega \ell^2}{\alpha_i}, \quad \rho_i = \frac{k_i}{k_1}, \quad \sigma = \frac{\mu \ell}{k_n}$$

Unless otherwise stated, in the remaining part of the paper we will drop the superscript star and refer to non-dimensional variables by using the same symbol as the corresponding dimensional ones.

3. Lumped parameters representation by thermal quadrupoles

A thermal quadrupole is a two ports lumped element that allow for the input to output representation of the heat flux (through) and the temperature (across) in a conducting body [10]. For the case of one-dimensional heat conduction the representation is obtained by taking the one-sided (with respect to time) Laplace transform of the system in equations (2). Therefore the initial-boundary values problem is mapped into a boundary values problem that depends on the Laplace variable s . The general solution of the transformed temperature is

$$U_i(s, x) = c_1^i(s) \cosh(x\sqrt{\beta_i s}) + c_2^i(s) \sinh(x\sqrt{\beta_i s})$$

where the constants c_1^i and c_2^i are determined by the boundary conditions.

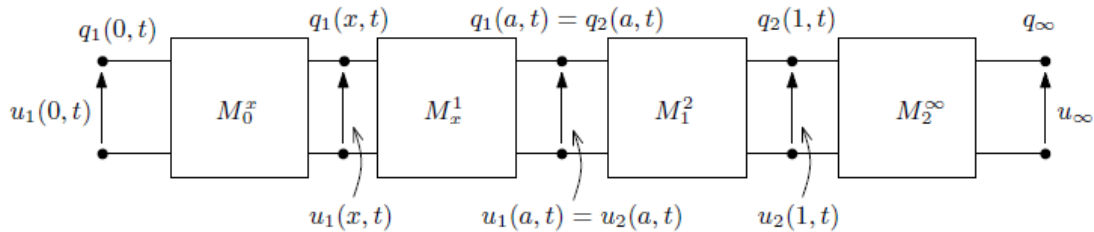


Fig. 2. Lumped parameters representation of the linear system (3) via thermal quadrupoles, with an observation point x located within layer 1. The case with observation point located in layer 2 can be easily obtained.

Given the linear constitutive relation between the heat flux and the temperature, it is possible to represent the one dimensional heat-conduction problem in terms of inputs and outputs of each layer, transformed by a suitable transition matrix whose entries are determined by the general solution above. For the system (2) the thermal quadrupoles block diagram is given in figure 2, with transition matrices given by

$$M_{i-1}^i = \begin{pmatrix} A_i & B_i \\ C_i & D_i \end{pmatrix}, \quad i = 1, 2, \dots, n \tag{3a}$$

$$A_i = D_i = \cosh\left((a_i - a_{i-1})\sqrt{\delta_i \beta_1 s}\right) \tag{3b}$$

$$B_i = \frac{1}{\rho_i \sqrt{\delta_i \beta_1 s}} \sinh\left((a_i - a_{i-1})\sqrt{\delta_i \beta_1 s}\right) \tag{3c}$$

$$C_i = \rho_i \sqrt{\delta_i \beta_1 s} \sinh\left((a_i - a_{i-1})\sqrt{\delta_i \beta_1 s}\right) \tag{3d}$$

where M_{i-1}^i is the transition matrix for the i -th layer that is used to represent the input to output behaviour of an homogeneous layer of thickness $a_i - a_{i-1}$, and

$$\delta_i = \frac{\beta_i}{\beta_1} = \frac{\alpha_1}{\alpha_i}$$

The transition matrices M_{i-1}^x and M_x^i are defined analogously by substituting a_i and a_{i-1} with x respectively. The transition matrix M_n^∞ which accounts for the convective boundary condition is given by

$$M_n^\infty = \begin{pmatrix} 1 & 1 \\ 0 & \sigma \end{pmatrix}$$

The nondimensional lumped parameters representation in Eqs. (3) implies that the transfer function depends on the excitation frequency ω through β_1 . In other words, the parameter β_1 is the nondimensional equivalent of ω .

We indicate with capital letters the Laplace transforms of fields introduced above. The input to output relation between the lumped variables U_1 and U_x , that is the temperature at the observation point x located in the i -th layer with respect to the input U_1 is obtained by solving the following system associated to the thermal quadrupoles representation of the system

$$\begin{pmatrix} U_1 \\ Q_1 \end{pmatrix} = M_0^1 M_1^2 M_2^3 \dots M_{i-1}^i \begin{pmatrix} U_x \\ Q_x \end{pmatrix} \tag{4a}$$

$$\begin{pmatrix} U_x \\ Q_x \end{pmatrix} = M_x^i M_i^{i+1} \dots M_{n-1}^n M_n^\infty \begin{pmatrix} U_\infty \\ Q_\infty \end{pmatrix} \tag{4b}$$

with $U_\infty = 0$. From Eqs. (4b) we obtain U_x and Q_x in terms of Q_∞ , which allows to obtain the relation between Q_x and U_x . Substitution into (4a) gives the relation between U_1 and U_x . The solution is in general represented by the following input to output relation which accounts for the geometry and the material properties

$$\frac{U_x}{U_1} =: G(s)$$

4. Approximate solution of the inverse problem

A closed form solution of the inverse problem, that is a closed form relation between β_1 and U_1 cannot be found. Here we approximate the transfer function $G(s)$ as the inverse of a power series expansion with respect to $\beta_1 s$ and assess the accuracy of the approximation for different cases. Specifically, $G(s)$ is approximated by

$$G(s) \sim G_a(s) = \frac{1}{\sum_{k=0}^N b_k (\beta_1 s)^k} =: \frac{1}{p_N(\beta_1 s)} \tag{5}$$

where coefficients b_k are given by

$$b_k = \frac{1}{k!} \left. \frac{\partial^k}{(\partial(\beta_1 s))^k} \left(\frac{1}{G(s)} \right) \right|_{\beta_1 s=0} \tag{6}$$

The approximated input to output relationship

$$\frac{U_x}{U_1} = G_a(s) = \frac{1}{p_N(\beta_1 s)}$$

allows to find an implicit solution of the inverse problem whenever the polynomial $p_N(\beta_1 s)$ is stable, that is whenever the roots have negative real part.

For a linear scalar system with transfer function $G_a(s)$ the response to the sinusoidal input $u_1(0, t) = \sin \omega t$ is given by $u_2(x, t) = |G_a(j\omega)| \sin(\omega t + \varphi)$, see for example [12, Chapter 7], where $|G_a(j\omega)|$ and φ are respectively the amplitude and the phase of the transfer function

$$|G_a(j\omega)|^2 = \Re(G_a(j\omega))^2 + \Im(G_a(j\omega))^2$$

$$\tan \varphi = \frac{\Im(G_a(j\omega))}{\Re(G_a(j\omega))}$$

where the operators \Re and \Im represent respectively the real and the imaginary part of their argument, and $j = \sqrt{-1}$. Therefore the amplitude of the temperature u_x at the observation point located at the non-dimensional abscissa x can be related to the nondimensional excitation frequency β_1 by

$$\Re(p_N(j\beta_1))^2 + \Im(p_N(j\beta_1))^2 = \frac{1}{|u_x|^2} \tag{7}$$

For $N = 2$ and $N = 3$ the explicit forms of Eq. (7) are respectively given by

$$b_0^2 - \frac{1}{|u_x|^2} + (b_1^2 - 2b_0b_2)\beta_1^2 + b_2^2\beta_1^4 = 0 \tag{8}$$

$$b_0^2 - \frac{1}{|u_x|^2} + (b_1^2 - 2b_0b_2)\beta_1^2 + (b_2^2 - 2b_1b_3)\beta_1^4 + b_3^2\beta_1^6 = 0 \tag{9}$$

The bi-quadratic structure of the expressions allows for the explicit solution to be found by using the formula for the roots of quadratic and cubic polynomials. Among the multiple roots, one must select the one such that β_1 is real and non-negative. We note that the implicit solution in (7) applies to multilayer systems provided that coefficients b_k are obtained for the specific materials and geometry. For a generic order N the implicit polynomial relation can be written as

$$b_0^2 + b_N^2\beta_1^{2N} + \sum_{k=1}^{N-1} (b_k^2 - 2b_{k-1}b_{k+1})\beta_1^{2j} - \frac{1}{|u_x|^2} = 0 \tag{10}$$

The solution for $N = 2$ is

$$\beta_1^2 = \frac{2b_0b_2 - b_1^2 \pm \frac{1}{|u_x|} \sqrt{|u_x|^2 b_1^2 (b_1^2 - 2b_0b_2) + 4b_2^2}}{2b_2^2} \tag{11}$$

In order to have $\beta_1^2 > 0$ for $|u_x| \rightarrow 0$ (β_1 would otherwise be complex, and so would be the frequency of excitation ω) we must select the solution

$$\beta_1^2 = \frac{2b_0b_2 - b_1^2 + \frac{1}{|u_x|} \sqrt{|u_x|^2 b_1^2 (b_1^2 - 2b_0b_2) + 4b_2^2}}{2b_2^2} \tag{12}$$

which gives

$$\beta_1 = \sqrt{\frac{2b_0b_2 - b_1^2 + \frac{1}{|u_x|} \sqrt{|u_x|^2 b_1^2 (b_1^2 - 2b_0b_2) + 4b_2^2}}{2b_2^2}} \tag{13}$$

The approximate solution in Eq. (13) holds provided that the argument of the radical is positive. For $N = 1$ we obtain the very simple formula

$$\beta_1 = \frac{1}{b_1} \sqrt{\frac{1}{|u_x|^2} - b_0^2} \tag{14}$$

In the following sections we give expressions for coefficients b_k corresponding to different scenarios. Coefficients are obtained with Mathematica[®].

4.1. Homogeneous slab

A homogeneous slab is characterized by $n = 1$ with the observation point x placed in the single layer. The first three coefficients that define the approximate transfer function G_a (for $N = 2$, that is second order truncation) are

$$b_0 = \frac{1 + \sigma}{1 + \sigma(1 - x)} \tag{14a}$$

$$b_1 = \frac{x}{6(1 + \sigma(1 - x))^2} (\sigma(\sigma + 1)x^2 - 3(\sigma + 1)^2 x + 2(\sigma(\sigma + 3) + 3)) \tag{14a}$$

$$b_2 = \frac{x}{360(1 + \sigma(1 - x))^3} (7\sigma^2(\sigma + 1)x^5 - 42\sigma(\sigma + 1)^2 x^4 + 5(19\sigma(\sigma(\sigma + 3) + 3) + 15)x^3 - 100(\sigma + 1)(\sigma(\sigma + 3) + 3)x^2 + 24(2\sigma(\sigma(\sigma + 5) + 10) + 15)x - 8(\sigma(\sigma(\sigma + 6) + 15) + 15)) \tag{14c}$$

For $x = 1$ and $\sigma = 0.08$ the plots of β_1 versus $|G_a(j\beta_1)| = |u_x|/U$ are shown in figures 3 for $N = 1$ (Eq. (14)) and $N = 2$ (Eq. (13)) respectively. The approximate solutions (dashed line and dashed-dotted lines) are compared with the exact solution (continuous line). The non-dimensional parameter σ is obtained by considering a slab of unit length with $k_1 = 49.8 \text{ W/(m K)}$ (carbon steel) and $\mu = 20 \text{ W/(m}^2 \text{ K)}$ (air).

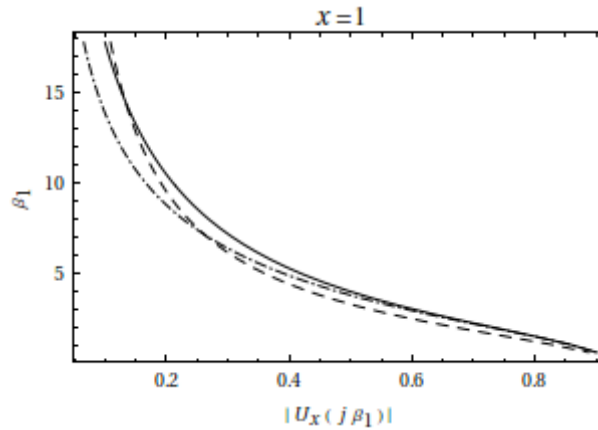


Fig. 3: Plots of β_1 versus $|U_x(j\beta_1)|$ from the analytical quadrupole solution (solid line), and the approximated polynomial solution with $N = 1$ (dashed line) and $N = 2$ (dot-dash line) for an homogeneous slab.

The relative percentage error $100|1 - \beta_1^a/\beta_1|$ is plotted in Fig. 4 for two values of N (Eqs (13) and (14)) and the same values of the non-dimensional parameter σ and x . For low amplitudes U_x the first order polynomial approximation gives lower errors than the second order polynomial approximation, whereas for the normalized amplitude approaching 1 the relative error of the second order approximation is considerably lower and monotonically decreases consistently with the plot in figure 3.

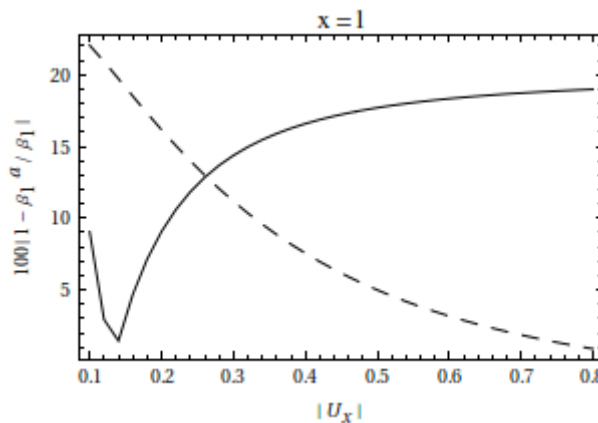


Fig. 4: Plots of the relative percentage error $100|1 - \beta_1^a/\beta_1|$ versus β_1 for $N = 1$ (solid line) and $N = 2$ (dashed line).

4.2. Two layer slab

We consider a two-layer slab ($n = 2$) with the observation point x at the interface mimicking a test to detect detachments between layers in a composite panel, see figure 1. The first three coefficients that define the approximate transfer function G_a (for $N = 2$) are

$$b_0 = 1 + \frac{\varrho_2 \sigma a_1}{\varrho_2 + \sigma(1 - a_1)} \tag{15a}$$

$$b_1 = \frac{a_1}{6(\varrho_2 + \sigma(1 - a_1))^2} (\sigma^2(3 - \varrho_2 - 2\varrho_2\delta_2)a_1^3 + \sigma(\sigma + \varrho_2)(6 - \varrho_2 - 6\varrho_2\delta_2)a_1^2 + 3(\sigma + \varrho_2)^2(1 - 2\varrho_2\delta_2)a_1 + 2\varrho_2\delta_2(3\varrho_2^2 + 3\varrho_2\sigma + \sigma^2)) \tag{15b}$$

$$\begin{aligned}
 b_2 = \frac{a_1}{360(\varrho_2 + \sigma(1 - a_1))^3} & \left(\sigma^3 \left((\varrho_2(3 + 4(5 - 2\delta_2)\delta_2)) - 15 \right) a_1^6 \right. \\
 & + \sigma^2(\varrho_2 + \sigma) \left((16\delta_2(3\delta_2 - 5) - 6)\varrho_2 + 45 \right) a_1^5 \\
 & - 3\sigma(\sigma + \varrho_2)^2 \left((40(\delta_2 - 1)\delta_2 - 1)\varrho_2 + 15 \right) a_1^4 \\
 & + 5 \left(12\varrho_2^4 \delta_2(2\delta_2 - 1) + \varrho_2^3(48\delta_2(2\delta_2 - 1)\delta_2 + 3) + 3\varrho_2^2\sigma(16\delta_2(2\delta_2 - 1)\sigma + 3) \right) a_1^3 \\
 & - 20\delta_2\varrho_2(\varrho_2 + \sigma)(6\delta_2 - 1)(3\varrho_2^2 + 3\varrho_2\sigma + \sigma^2) a_1^2 \\
 & \left. + 24\delta_2^2\varrho_2(15\varrho_2^3 + 20\varrho_2^2\sigma + 10\varrho_2\sigma^2 + 2\sigma^3) a_1 - 8\delta_2^3\varrho_2(15\varrho_2^3 + 15\varrho_2^2\sigma + 6\varrho_2\sigma^2 + \sigma^3) \right)
 \end{aligned} \tag{15c}$$

The plot in figure 5 shows the first order (dashed line) and second order (dot-dash line) approximate solutions versus the analytical quadrupoles solution (continuous line). Values of non-dimensional parameters used to compute the coefficients in Eqs. (15) are

$$\begin{aligned}
 a_1 = 0.5, \quad \varrho_2 = 5.02, \quad \delta_2 = 0.133, \\
 \sigma = 0.08, \quad x = a_1
 \end{aligned} \tag{16}$$

The set of parameters has been obtained by considering material 1 and material 2 to be, respectively, carbon steel and aluminum.

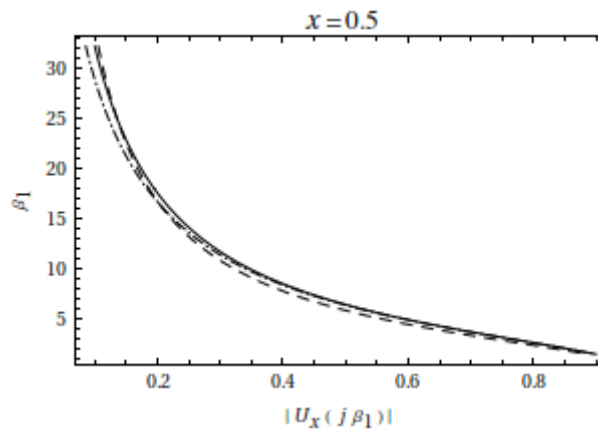


Fig. 5: Plots of β_1 versus $|U_x(j\beta_1)|$ from the analytical quadrupole solution (solid line), and the approximated polynomial solution with $N = 1$ (dashed line) and $N = 2$ (dot-dash line) for a two layer slab.

The relative percentage error $100|1 - \beta_1^a/\beta_1|$ is plotted in Fig. 6 for two values of N (Eqs (13) and (14)) and the same values of the non-dimensional parameters. For low amplitudes U_x the first order polynomial approximation gives lower errors than the second order polynomial approximation, whereas for the normalized amplitude approaching 1 the relative error of the second order approximation is lower. The simple first order approximation in Eq. (14) allows in this case to estimate the non-dimensional excitation frequency β_1 within a maximum error of about 10%.

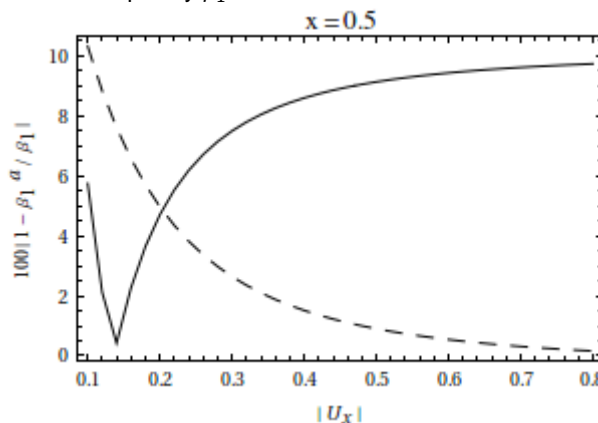


Fig. 6: Plots of the relative percentage error $100|1 - \beta_1^a/\beta_1|$ versus β_1 for $N = 1$ (solid line) and $N = 2$ (dashed line) (Two layer slab).

4.1.1. Dimensional example

We consider a two layer slab with the same parameters as above. To estimate the frequency of excitation ω we use the first order approximation in Eq. (14). From the definition of β_1 we obtain the dimensional formula

$$\omega = \frac{\alpha_1 \beta_1}{\ell^2} = \frac{\alpha_1}{\ell^2 b_1} \sqrt{\frac{1}{|u_x|^2} - b_0^2} \quad (17)$$

For a carbon steel we have $\alpha_1 = 1.34 \times 10^{-5} \text{m}^2 \text{s}^{-1}$ Moreover for the non-dimensional parameters in Eq. (16) (obtained by considering carbon steel and aluminum as materials for the two layer slab) we have the following expressions for b_0 and b_1 in terms of $x \in [0,1]$

$$b_0 = \frac{5.26}{5.1 - 0.08x} \quad (17a)$$

$$b_1 = \frac{6.23 + 3.42x - 1.79x^2 + 0.00936x^3}{(5.1 - 0.08x)^2} \quad (17b)$$

For $x = a_1 = 0.5$ and $\ell = 1\text{m}$ the plot of ω versus $|u_x|/U$ (Eq. (17)) is given in Fig. 7.

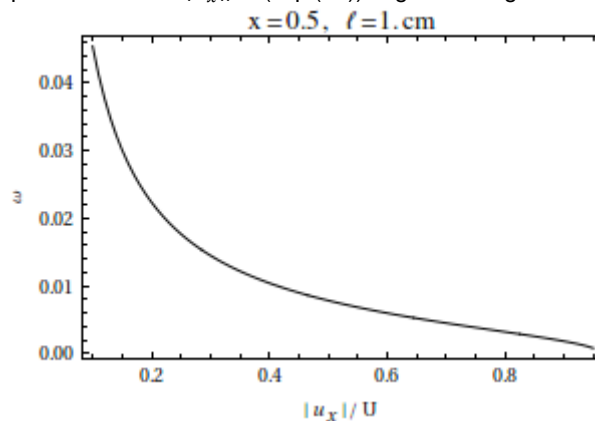


Fig. 7: For a two layer slab comprised of carbon steel and aluminum, plot of the frequency of excitation ω versus $|u_x|/U$.

5. Summary

We derived a polynomial implicit solution of the inverse heat conduction problem in a multi-layer slab. The solution is based on a lumped parameters representation of the initial-boundary values heat conduction problem by means of thermal quadrupole method. By consider the temperature at the excited boundary and in one point along the thickness as input and output, we considered the Taylor series approximation of the transcendental quadrupoles transfer function for the implicit polynomial representation of the inverse problem. A simple approximated formula based on first order truncation is given and the error with respect to the analytical solution is computed for homogeneous and bi-material slab. The first order approximation can be an effective design tool for infrared non-destructive testing when the solution of the inverse problem is required.

REFERENCES

- [1] M. Joensson, B. Rendahl, and I. Annergren, "The use of infrared thermography in the corrosion science area," *Materials and Corrosion-Werkstoffe und Korrosion*, vol. 61, no. 11, pp. 961–965, NOV 2010.
- [2] C. Meola and G. M. Carlomagno, "Impact damage in GFRP New insights with infrared thermography," *Composites Part A-Applied Science and Manufacturing*, vol. 41, no. 12, pp. 1839–1847, DEC 2010.
- [3] C. Meola, G. M. Carlomagno, D. Annicchiarico, M. Giordano, and M. Zarrelli, "Detection of delamination in carbon-fibre-reinforced polymers with lock-in thermography," *Proceedings of the Institution of Mechanical Engineers Part G-Journal of Aerospace Engineering*, vol. 224, no. G11, pp. 1219–1227, 2010.
- [4] L. Junyan, W. Yang, and D. Jingmin, "Research on thermal wave processing of lock-in thermography based on analyzing image sequences for NDT," *Infrared Physics & Technology*, vol. 53, no. 5, pp. 348–357, SEP 2010.
- [5] G. Gralawicz, J. Wo'ny, G. Owczarek, and B. Wiecek, "Detecting flaws in composite material-thermal model and simulation results," in *9th International Conference on Quantitative InfraRed Thermography (QIRT 08)*, Krakow (Poland), July 2-5 2008.
- [6] N. Rajic, "Principal component thermography for flaw contrast enhancement and flaw depth characterisation in composite structures," *Composite Structures*, vol. 58, no. 4, pp. 521–528, DEC 2002.

- [7] V. S. Ghali, N. Jonnalagadda, and R. Mulaveesala, "Three-Dimensional Pulse Compression for Infrared Nondestructive Testing," *IEEE Sensors Journal*, vol. 9, no. 7, pp. 832–833, JUL 2009.
- [8] P. J. Shull, *Nondestructive Evaluation: Theory, Techniques, and Applications*. CRC Press, 2002.
- [9] D. Neculescu, D. Spinello, E. Borazjani, and S. Bayat, "Analytical and simulation investigation of the experimental design for infrared nondestructive testing," in *Control Automation (IEEE MED), 2011 19th Mediterranean Conference on*, June 2011, pp. 946–951.
- [10] D. Neculescu, S. Bayat, and M. Eghtesad, "IR Non Destructive Testing Experiment Design," in *10th International Conference on Quantitative InfraRed Thermography (QIRT 10), Qu´bec (Canada), July 27-30 2010*.
- [11] D. Maillet, S. André, J. C. Batsale, A. Degiovanni, and C. Moyne, *Thermal Quadrupoles: Solving the Heat Equation through Integral Transforms*. Wiley, 2000.
- [12] K. Ogata, *Modern Control Engineering*. Prentice Hall, 2009.